2016

Search for Electroweak Production of Supersymmetric Particles with two photons, an electron, and missing transverse energy

Paul Myles Eugenio

A SEARCH FOR ELECTROWEAK PRODUCTION OF SUPERSYMMETRIC PARTICLES WITH TWO PHOTONS, AN ELECTRON, AND MISSING TRANSVERSE ENERGY

Paul Eugenio

A thesis submitted to the
Florida State University
Department of Physics
in partial fulfillment of the requirements for graduation with
Honors in the Major

Spring 2016

Dr Andrew Askew
Thesis Director

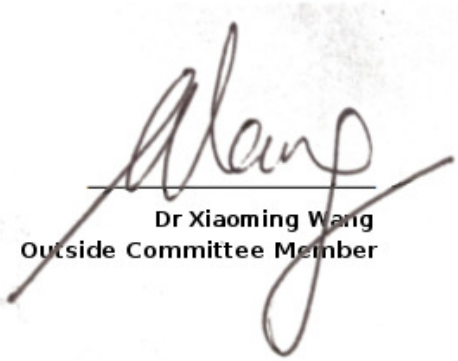

Dr Xiaoming Wang
Outside Committee Member

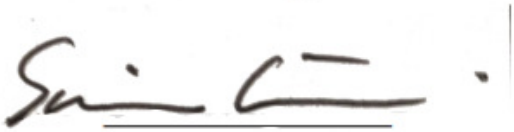

Dr Simon Capstick
Committee Member

Abstract

A search for Supersymmetry (SUSY) using a final state consisting of two photons, an electron, and missing transverse energy. This analysis uses data collected by the Compact Muon Solenoid (CMS) detector from proton-proton collisions at a center of mass energy $\sqrt{s}$ =13 TeV. The data correspond to an integrated luminosity of 2.26 fb^{-1}. This search focuses on a R-parity conserving model of Supersymmetry where electroweak decay of SUSY particles results in the lightest supersymmetric particle, two high energy photons, and an electron. The lightest supersymmetric particle would escape the detector, thus resulting in missing transverse energy. No excess of missing energy is observed in the signal region of MET>100 GeV. A limit is set on the SUSY electroweak Chargino-Neutralino production cross section.

Contents

List of Figures

List of Tables

1 Introduction

.

The Standard Model of Particle Physics (SM) is a description of all known elementary (point-like) particles and describes three fundamental forces of nature. These forces – strong, electromagnetic, and weak – are mediated by "force carriers" (gauge bosons) which have integer spin. Another field, the Higgs field – along with its associated boson, the Higgs boson – is the mechanism by which fundamental particles get their mass. Along with these bosons, the Standard Model describes the interaction of particles with half-integer spins (fermions). These particles constitute what we commonly call matter, and are broken up into two classes: leptons and quarks. Leptons include particles such as the electron – a principle component to atomic and molecular physics – and its heavier cousins, the muon and tau. Quarks are the bricks that build subatomic protons and neutrons that define nuclear physics, as well as other bound states of quarks (hadrons). The collection of all these particles, the Standard Model, is a successful description of particle physics; however, there are still many open questions that lead physicists to suspect it may be incomplete.

Some of the strongest evidence for the incompleteness of the Standard Model comes from cosmology and the Cosmic Microwave Background (CMB). The standard model of cosmology, the Λ Cold Dark Matter model (ΛCDM), relates the curvature of the universe to its matter-energy composition. Analyses done of the CMB by the Wilkinson Microwave Anisotropy Probe (WMAP) determined the observable universe is flat [1], and thus the matter-energy composition of the universe is as described by Fig(1). This suggests the strong possibility that the SM only describes 4.6% of what is to be described.

Figure 1: WMAP Matter-Energy Composition of Observable Universe [2]

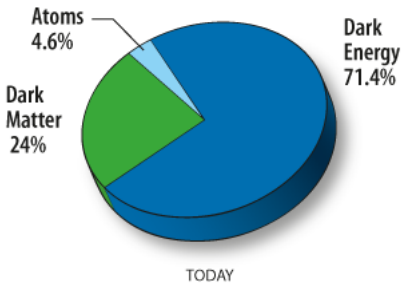

This and other suspicions drive the construction of new theories and extensions to the Standard Model as it stands today. The focus of this analysis, Supersymmetry (SUSY), predicts new particles commonly referred to as "supersymmetric particles", or "SUSY particles". Further, SUSY predicts new massive, weakly interacting, and stable particles – excellent candidates for dark matter – which could be measured if produced in our detector.

1.1 Weakly Interacting Massive Particles

.

Observations of visible matter on the cosmological scale has lead to mounting evidence for the existence of dark matter. The earliest evidence comes from galactic rotation speeds, where matter observed far from the galactic center moves faster than predicted for the visible matter distribution.

$$v(r) \propto \sqrt{\frac{M(r)}{r}} \tag{1}$$

Eqn(1) predicts the velocity of an object at a distance r from the center of a mass distribution $M(r)$. For a matter distribution that reaches out to a distance R the mass

distribution takes on a maximal constant value $M(R)$. Thus for regions outside the mass distribution our velocity distribution $v(r)$ takes on the form (2).

$$v(r) \propto \sqrt{\frac{1}{r}} \tag{2}$$

If this is true then the velocity distribution of the most distance stars in the galaxy should drop off with the reciprocal of the square-root of their distance from the galactic center; however, this is in clear contradiction to observation, where the velocities of most distant stars are seen to stay constant for increasing r. This predicts that the matter distribution $M(r)$, which takes into account all visible matter in the galaxy, is incorrect.[3]

Since these initial observations, a wealth of other evidence has amassed in support of dark matter. These observations make use of gravitational lensing [4] to find and map the distribution of dark matter in a number of systems. Using a similar approach to the one outline above, one can sum the visible matter in a system and show a deficit required to produce the observed gravitational lensing.

Figure 2: Bullet Cluster [5]

An analysis of gravitational lensing in two colliding galaxy clusters, known as the Bullet Cluster (1E 0657-558), shows an offset of the center of mass for visible matter (colored red) to the observed center of mass of the entire system (colored blue). Further, the dark matter passes through itself, in stark contrast to the gas which loses velocity in the collision. The fact that it did not interact with itself in any observable way is strong support for the weakly interacting nature of dark matter.

1.2 SUSY

.

Supersymmetry (SUSY) extends the Standard Model to include new supersymmetric particles. These particles are partners to SM particles, having identical quantum numbers but differing in intrinsic spin. Thus every SM boson/fermion has a SUSY fermion/boson partner respectively. This picture, however, is incomplete in that it predicts SUSY and SM partners to have the same mass. If this were true, previous

experiments would have produced and discovered these supersymmetric partners. For SUSY particles to exist they must have larger masses than their SM partners, and thus would require higher center of mass accelerator energies to produce. This suggests some symmetry breaking mechanism[1] by which SM and SUSY particles have different masses.

A particular family of supersymmetric models, considered to be R-Parity Conserving, requires the conservation of a quantity (R-Parity) that prevents supersymmetric particles from decaying into a final state solely comprised of Standard Model particles. As a result, the lightest supersymmetric particle would be stable, massive, and likely to interact only via the weak-force. Thus such a particle would be a Weakly Interacting Massive Particle (WIMP) and a likely candidate for dark matter. If discovered it would have a profound impact on our understanding of the structure of the universe as a whole. Further, R-parity conservation is integral in providing a model of Supersymmetry in which the proton does not decay. Models that do not conserve R-parity lead to a decaying proton and thus prevent stable hydrogen ions from forming. This is in clear contradiction of reality, and thus necessitates R-parity conservation.

The particular physics we are searching for is an R-parity conserving model, which provides a mechanism for electro-weak production of stable Supersymmetric particles. This model contains a decay process in which an off-shell W boson decays into a chargino (charged supersymmetric particle) and neutralino (neutral supersymmetric particle). The neutralino subsequently decays into the lightest supersymmetric particle along with a high energy photon. The chargino decays into a W boson and a neutralino; the latter which further decays into a second high energy photon and a second lightest supersymmetric particle. The W boson decays into a high energy electron and a neutrino.

[1]Symmetry breaking has observed to occur in nature already. Broken symmetries occur in condensed matter systems [6], and are critical elements of the electro-weak unification in particle physics.

The kinematics of the final state particles depend on the mass, or rest energy, of the intermediate supersymmetric particles.

Figure 3: Feynman Diagram showing final state of two photons plus lepton plus MET

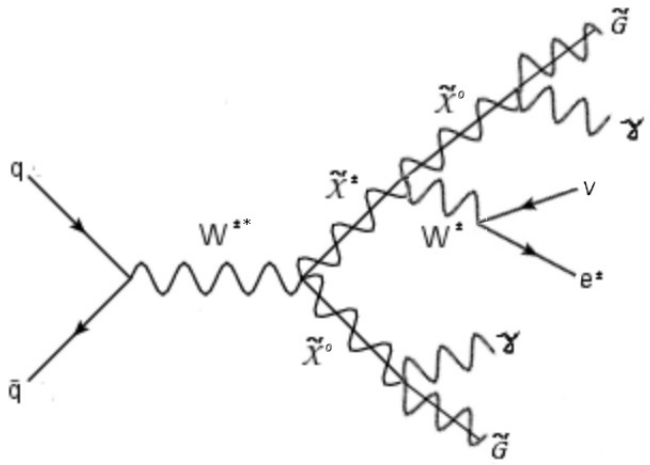

Prior searches for Supersymmetry have been made using lower center-of-mass energies (8 TeV) at the LHC, with a focus on strong production of SUSY particles.[2] No evidence of Supersymmetry was found in these earlier searches. This search makes use of data collected at the Compact Muon Solenoid (CMS) detector at the LHC with center-of-mass collision energies of 13 TeV. This search is unique in that it contains data with the signature of missing transverse energy, two high energy photons, and a high energy lepton.

[2]Ref[7] is an example of an electro-weak search at 8 TeV. Ref[8] is an example of an electro-weak search using a final state of one photon and one lepton at 8 TeV. Neither show evidence of Supersymmetry.

2 CMS Detector

.

Data used in this analysis were taken by the Compact Muon Solenoid (CMS) detector at the Large Hadron Collider in CERN, Switzerland. The detector is composed of 4 subdetectors – a silicon tracker, electromagnetic calorimeter (ECAL), hadronic calorimeter (HCAL), and muon chambers. Each subdetector is specialized to measure the characteristics and kinematic properties of particles produced in a collision.

The origin of the name Compact Muon Solenoid is a large 3.8 Tesla superconducting solenoid. The solenoid encompasses the silicon tracker, ECAL, and HCAL. The magnetic field causes charged particles to move along curved trajectories with radius R defined in Eqn(3). Where p is the momentum of the particle, q the charge, and B the magnetic field.

$$R = \frac{p}{qB} \tag{3}$$

The silicon tracker, measures electrical signals produced by charged particles in order to track their motion and determine the radius of their trajectory. Electrical signals are produced when charged particles pass through each layer of the silicon tracker, depositing ionization energy, and producing electron-hole pairs which are then measured by electrodes [9]. Hits in the silicon tracker are formed together into helical tracks used in particle reconstruction.

Outside the silicon tracker are two calorimeters, the ECAL and HCAL. Both are designed to measure energy depositions from particles produced in events. The HCAL

is made out of material with high atomic mass number A, thus increasing the likely hood of hadronic interactions; the ECAL utilizes materials with a high atomic number Z to increase the likely-hood of electromagnetic interactions. As their names suggest, the HCAL is designed to measure hadrons while the ECAL is designed to measure electromagnetic objects (electron, photons, etc). Outside the superconducting solenoid are the muon chambers, which allow for very accurate identification of muons.

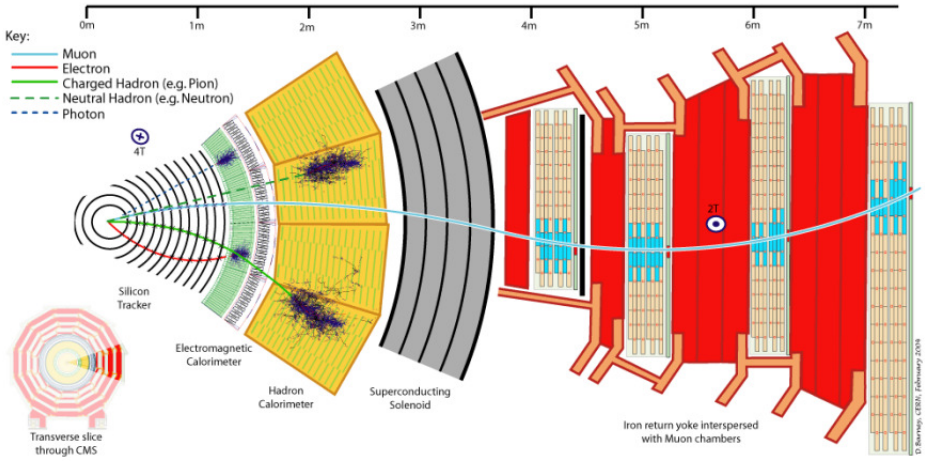

Figure 4: Transverse Slice of CMS Detector showing how different particles interact with the subdetectors to give a unique signature [10]

The key particles in this search – photon and electron – are measured using the silicon tracker and ECAL. Electrons are charged particles which move in curved trajectories due to the magnetic field, leaving hits in the silicon tracker. Photons carry no charge and are not affected by the magnetic field; ideally only leaving a signature in the ECAL.

3 Data

3.1 Particle Flow and Reconstruction

.

It is impossible to say with absolute certainty that a photon (or any particle) was detected in the detector. At the most fundamental level the detector measures hits in the silicon tracker and energy deposited in the calorimeters. From these fundamental measurements one can introduce a hypothesis that those hits in the silicon form a unified track, or that the energy deposited in a calorimeter is associated together into one cluster of energy. From these logical elements – tracks and clusters – one can further hypothesize and combine them into reconstructed particles.[3]

Reconstruction not only provides us with a necessary hypothesis for what a photon is, or what an electron is, but further provides us with important quantities – shower shape, isolation, H/E – used in selecting the candidate sample.

Missing energy, the key search signature of this event, is tied to the precision to which the detector can measure all of the energy of an event. Particle Flow MET provides both the magnitude and direction of MET in the event.

3.1.1 ECAL Clustering and R9

.

In the ECAL local depositions of energy can be logically grouped into clusters under the hypothesis that they represent an electromagnetic shower. These clusters are logical

[3]The full details of reconstruction are outside the scope of this analysis. For a brief but excellent description of particle reconstruction see Ref[12].

objects which, under a further hypothesis that they originate from the same electromagnetic particle produced in a collision, can be grouped into superclusters [14].

R9 is defined as the ratio of the energy deposited in a 3x3 grid of crystals E_{3x3} to the energy deposited in the supercluster E_{SC}, where the 3x3 grid is centered around the highest energy crystal in the cluster. It represents the lateral spread of energy from an electromagnetic shower [12]. R9 is mathematically represented by Eqn(4).

$$R9 = \frac{E_{3x3}}{E_{SC}} \tag{4}$$

R9 is not used as a selection criteria for this analysis; however, an R9 cut is required by the trigger and thus included here for completeness.

3.1.2 Conversion Safe Electron Veto

.

Reconstructed photon and electron objects are very similar. Both are reconstructed from superclusters in the ECAL, but with reconstructed electrons requiring an associated track. Further, photons can decay into electron-positron pairs. These "conversion" still represent a photon that was produced at the primary vertex (and thus of interest to this analysis).

Electron pairs coming from the decay of an energetic photon will likely have a conversion vertex displaced from the primary vertex, and thus have missing inner hits in the silicon tracker. The Conversion Safe Electron Veto is a check against incorrect pairings of unrelated electrons as a single converted photon. It checks whether the electron pair has a good vertex, is displaced from the primary vertex, and has missing inner hits in

the tracker [12, 15].

3.1.3 Shower Shape

.

Shower shape is a key element in identifying photons. Both jets and photons leave energy deposited in the electromagnetic calorimeter; however, jets are composed of multiple particles and thus tend to leave a broader energy deposition.

The shower width $\sigma_{i\eta i\eta}$ is defined using the variance in η (5). A logarithmic weighting is used (6) because electromagnetic showers are assumed to have a Gaussian falloff [16].

Equation(5) is a sum over all crystals in a 5x5 grid in the ECAL, where $\bar{\eta}$ is the energy weighted mean η of the shower, η_i is the η of the i^{th} crystal, and W_i is the logarithmic weight on the i^{th} crystal defined in Eqn(6). In Eqn(6) E_i and E_{5x5} represent the energy deposited in the i^{th} crystal and in the 5x5 grid of crystals respectively. W_0 is a dimensionless free parameter that must be optimized [11, 16].[4]

$$\sigma^2_{i\eta i\eta} = \frac{\Sigma_{5x5} W_i (\bar{\eta} - \eta_i)^2}{\Sigma_{5x5} W_i} \tag{5}$$

$$W_i = max(0, W_0 + \log(\frac{E_i}{E_{5x5}})) \tag{6}$$

[4]The shower shape and the logarithmic weighting Eqn(6) is detailed in the original paper Ref[16].

3.1.4 Isolation

.

Hadron fragmentation is the process by which high energy hadrons split into more hadrons in order to produce a colorless state. The resulting jet of hadrons have the potential to deposit energy in both the hadronic and electromagnetic calorimeter, and can also produce and be accompanied by other particles (including photons and electrons).

We hypothesize that objects measured in close proximity to one another are likely to have originated from a jet of hadrons. Isolation variables are employed in order to discern between particles originating from jets and those of interest to this analysis.

Objects are required to have an angular separation ΔR greater then 0.3 between themselves and any other object (lead photon, trail photon, electron) in the event. ΔR is defined by Eqn(7), where $\Delta\phi$ and $\Delta\eta$ are the differences between the two objects in the azimuthal angle ϕ and the pseudorapidity η respectively.

$$\Delta R = \sqrt{(\Delta\phi)^2 + (\Delta\eta)^2} \tag{7}$$

$$\Delta\phi = \phi_1 - \phi_2 \tag{8}$$

$$\Delta\eta = \eta_1 - \eta_2 \tag{9}$$

The ρ-correction is a correction to the sum p_T calculated by the particle flow iso-

lation cones for energy contamination due to the underlying event. Objects must pass a ρ-corrected charged hadron isolation, neutral hadron isolation, and photon isolation cut. Every event has a characteristic ρ, which is a measure of the average energy density for that event, and has units of momentum divided by area $[\frac{p_T}{A}]$. The sum p_T in the isolation cones is corrected by subtracting ρ times an effective area that varies with position η in the barrel [12].

Isolation Criteria
Charge Hadron Isolation < 2.51
Neutral Hadron Isolation $< 21.11 + .0065 * p_{T_{photon}}$
Photon Isolation $< 3.70 + .0032 * p_{T_{photon}}$

Table 1: ρ-corrected Particle Flow Isolation Criteria for both lead and trail photons

3.1.5 H/E

.

H/E is a measure of the ratio of energy deposited in the hadronic calorimeter to the electromagnetic calorimeter directly behind the core of the electromagnetic shower. This quantity allows us to remove neutral and charged hadrons from the candidate sample. Charged hadrons are likely to leave energy in both the electromagnetic calorimeter and the hadronic calorimeter, and neutral hadrons are most likely to deposit their energy in the hadronic calorimeter. These signatures are distinct from the candidate photons, which deposit the majority of their energy solely in the electromagnetic calorimeter.

3.2 Datasets and Trigger

.

The data used in this analysis corresponds to an integrated luminosity of 2.26 fb^{-1}.

The trigger used in this analysis was developed for the search for Higgs decays to two photons ($H^0 \rightarrow \gamma\gamma$). This is the same trigger used by the CMS diphoton search for gauge-mediated SUSY [13]. A primary question of this analysis is how the analysis is affected by the requirement of an electron, in comparison with the analysis in which only two photons are required.

This candidate diphoton trigger requires the lead photon and trail photon to have E_T greater than 30 GeV and 18 GeV respectively, and a combined invariant mass greater than 95 GeV. Further, photons are required to pass an H/E and loose R9 cut, and are required to pass either a tight R9 cut or isolation and shape cuts.[5]

The control sample used in the QCD background estimation was selected using a trigger nearly identical to the diphoton trigger, but requiring the electrons both be matched to a pixel seed and have a combined invariant mass greater than 70 GeV.

[5]It should be noted that this trigger set does not require objects to be in the barrel, and even has requirements to trigger on objects that hit in the endcap; however, this analysis only selects photons measured in the barrel.

3.3 Monte-Carlo Simulation

.

In order to account for all kinematic possibilities, we use a Monte-Carlo simulation of a grid of possible mass values in the region where the chargino mass is greater than the neutralino. This region is chosen to ensure that the chargino will decay into the neutralino, and that the hypothesized decay process can occur.

The six mass point chosen are listed in Table(2). There corresponding cross sections are driven almost entirely by the chargino mass, and are listed in Table(3).

$m_{\chi_\pm}$ [Gev]	m_{χ_0} [GeV]
400	300
500	300
500	400
600	300
600	400
600	500

Table 2: Mass Points

$m_{\chi^\pm}$ [GeV]	Cross Section [fb]
400	121.013 +/- 9.61659
500	46.3533 +/- 4.16461
600	20.1372 +/- 2.04438

Table 3: Chargino Mass and Cross Section

Monte-Carlo is also vital in crafting selection cuts, determining acceptances, and provides us a model for understanding the shape of our signal and how it interacts with the detector. This is because the simulation provides complete information on both the physics being generated and how it interacts with the detector. The ratio of which – number of events that pass selection criteria divided by the total number of known

generated events – is the efficiency for those selection criteria.

This gives us insight into how our selection criteria affects the hypothesized supersymmetric decay process of interest; however, we do not fully trust simulation alone. We adapt an approach in which all selection criteria are crafted in simulation and tested on data to maximize efficiency. This wards against selection criteria that, while efficient in simulation, cut away a substantial fraction of the candidate sample.

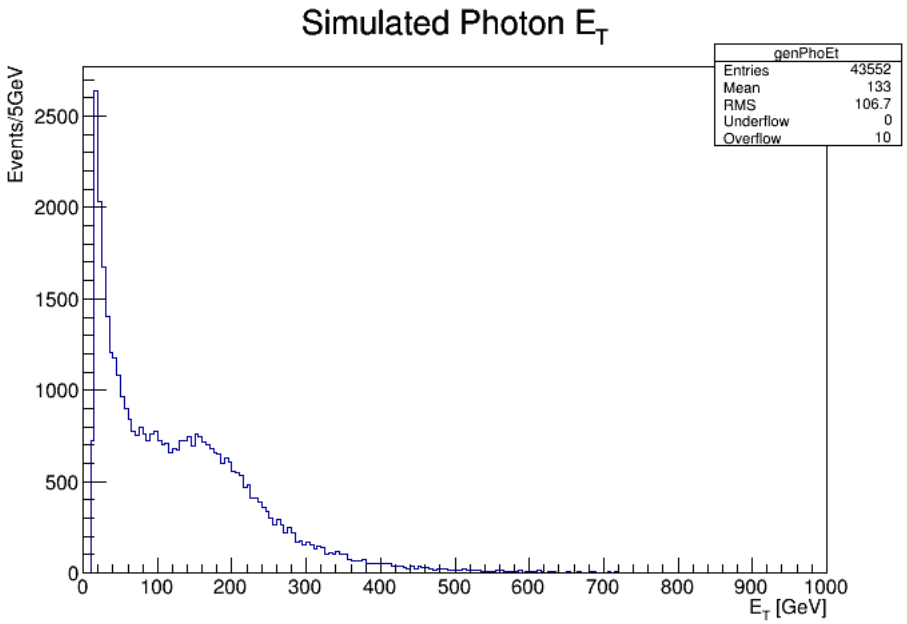

Figure 5: Photons generated by simulation corresponding to a chargino and neutralino mass of 500 GeV and 400 GeV respectively.

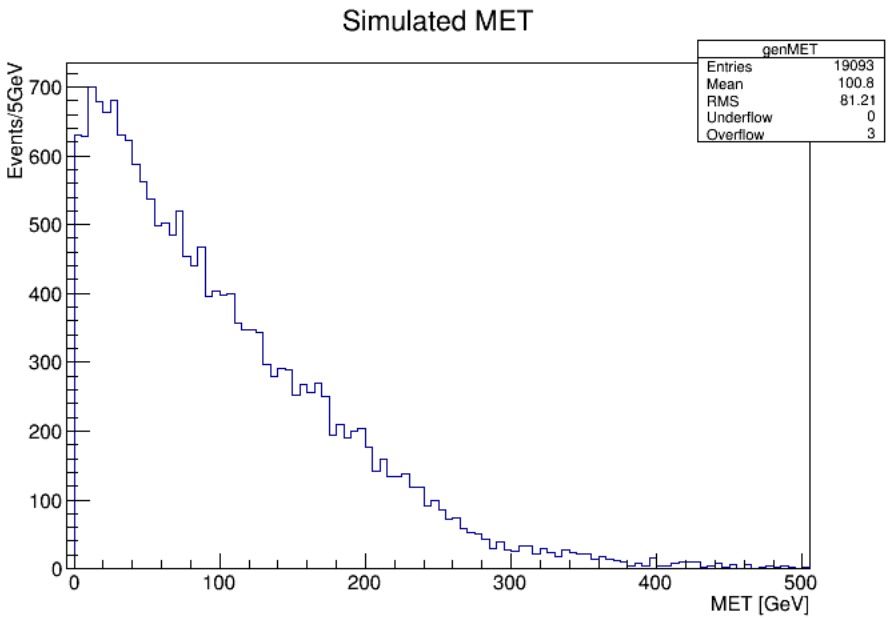

Figure 6: Generator Level MET corresponding to a chargino and neutralino mass of 500 GeV and 400 GeV respectively.

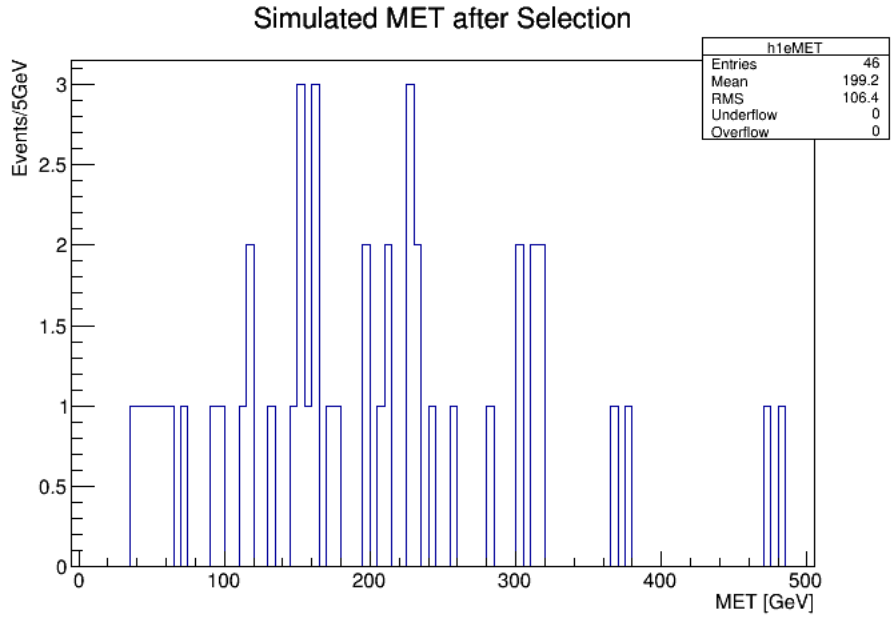

Figure 7: Generated MET after selection corresponding to a chargino and neutralino mass of 500 GeV and 400 GeV respectively.

4 Selection

.

To best assure that our data is an accurate description of new physics of interest to this analysis, we need to introduce a number of selection criteria, or selection cuts, on our sample data set (two photons plus electron plus MET). This narrowing of the data sample removes[6] events unrelated to the search – primarily Standard Model processes (background) that make up the largest fraction of the initial data set. The resulting post-selection candidate is then further analyzed in Background Estimation.

The selection criteria used here require two high energy photons and a high energy electron. The highest energy photon and the second highest energy photon in the event are labelled "lead photon" and "trail photon" respectively.

4.1 Candidate Photons

.

This analysis implements a "loose" selection criteria for both the lead and trail candidate photons. These criteria were designed as part of a set of robust CMS Run 2 selection criteria, which are as follows:

1) All photons are required to be within the barrel. This requirement is fulfilled by photons with a pseudorapidity less than 1.44 ($|\eta| < 1.44$).

2) Leading energy photons are required to have E_T >30 GeV. Trailing energy pho-

[6]There is an associated efficiency with each selection cut that represents the lose of "good" events due to cutting. Selection criteria are modelled and crafted using Monte-Carlo for this reason.

tons are required to have E_T >25 GeV.

3) Photons must pass the Conversion Safe Electron Veto.

4) Signal shape requirements for photons are such that H/E<.0559 and $\sigma_{i\eta i\eta}$ <.0100 .

5) Photons are also required to pass isolation criteria Table(1).

6) Events are only selected if all objects are outside a cone of $\Delta R > .3$, where ΔR is the absolute angle between all objects.

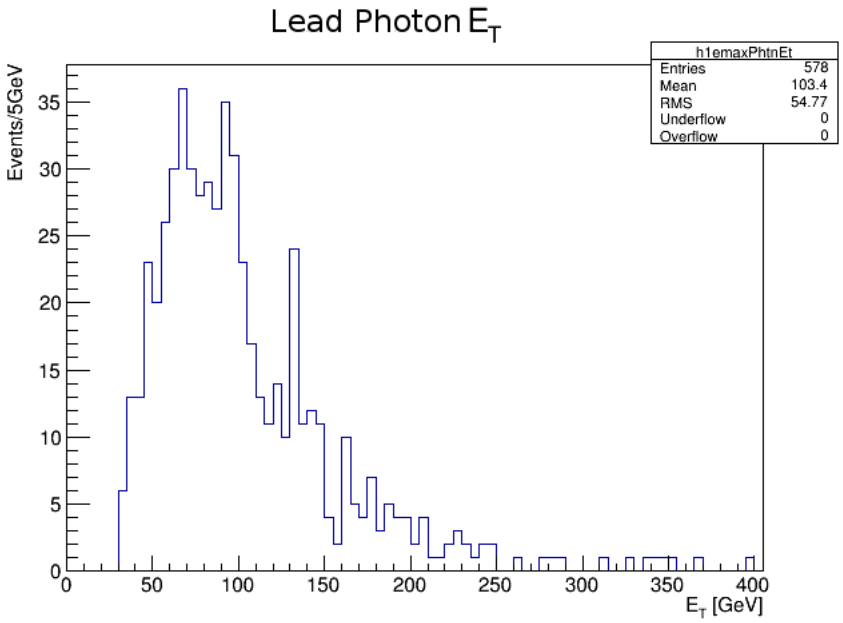

Figure 8: Lead Photon E_T

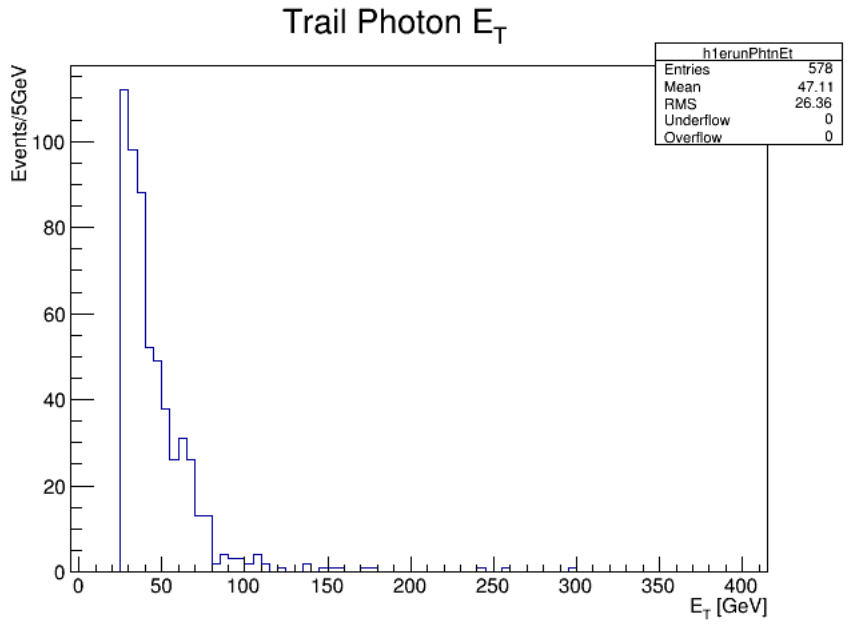

Figure 9: Trail Photon E_T

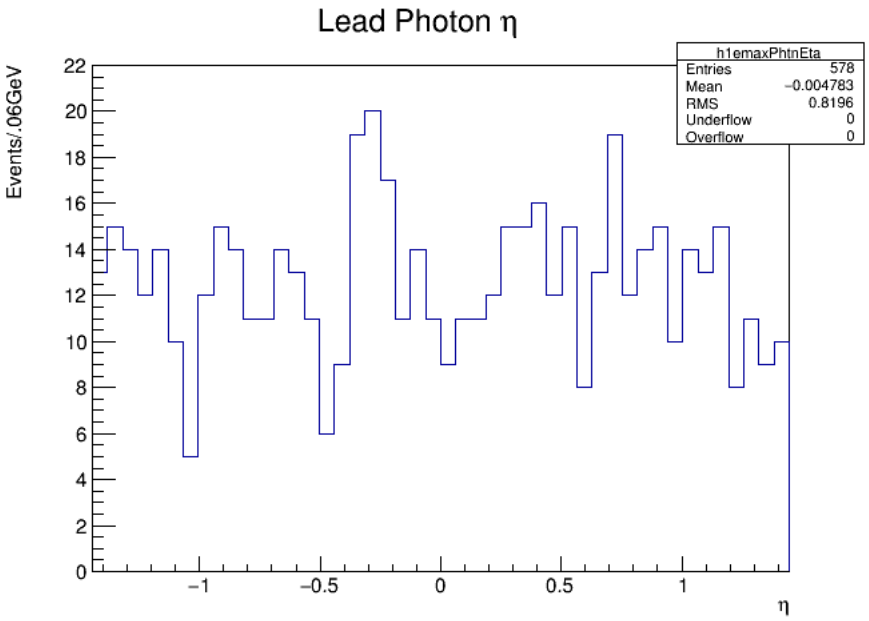

Figure 10: Lead Photon Pseudorapidity η

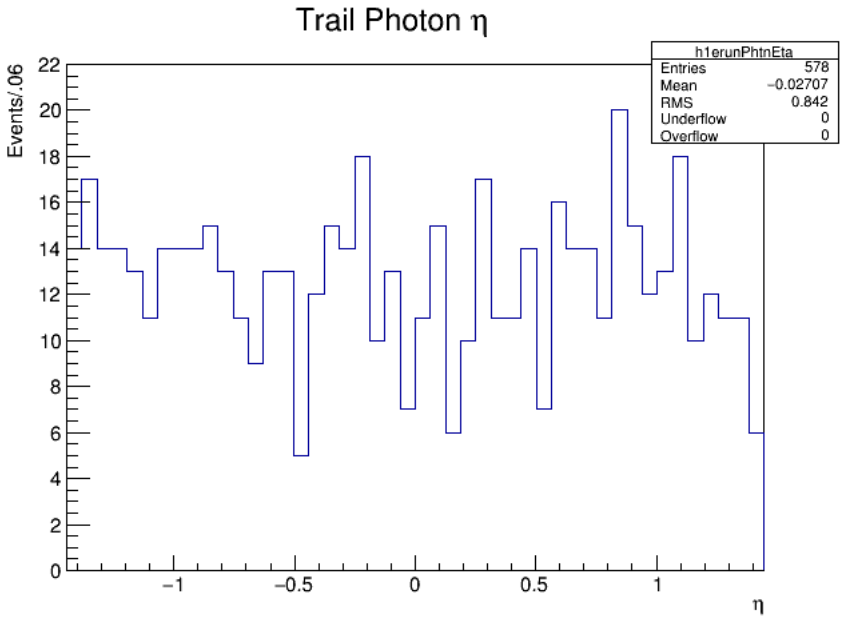

Figure 11: Trail Photon Pseudorapidity η

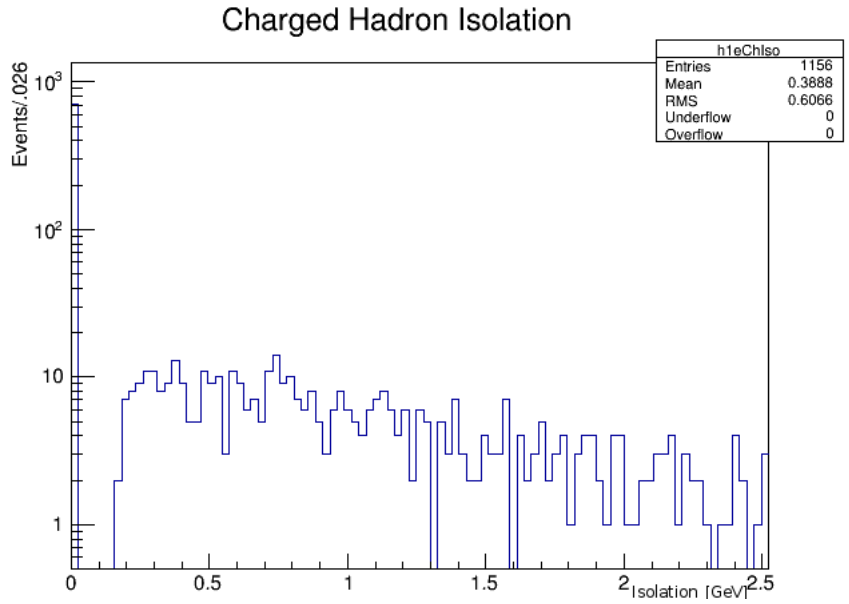

Figure 12: Charged Hadron Isolation for both lead and trail photons

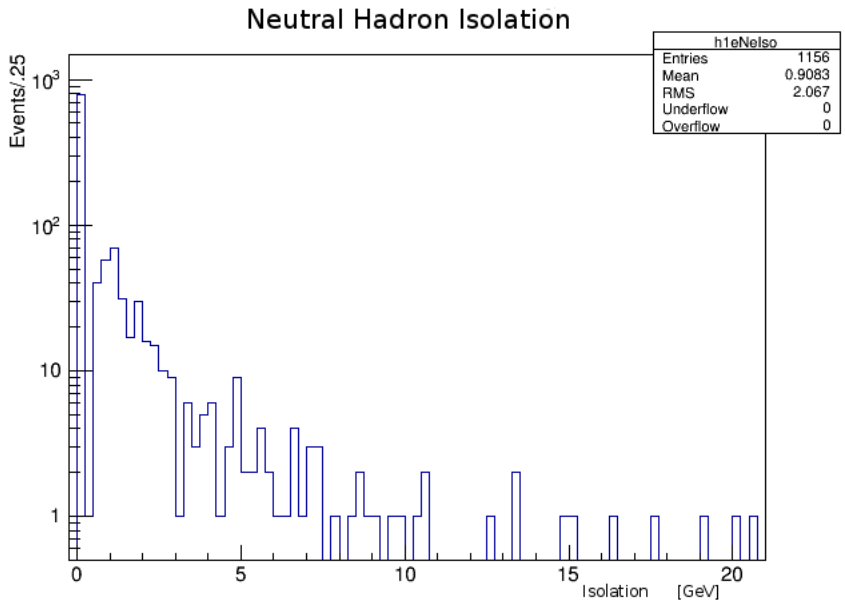

Figure 13: Neutral Hadron Isolation for both lead and trail photons

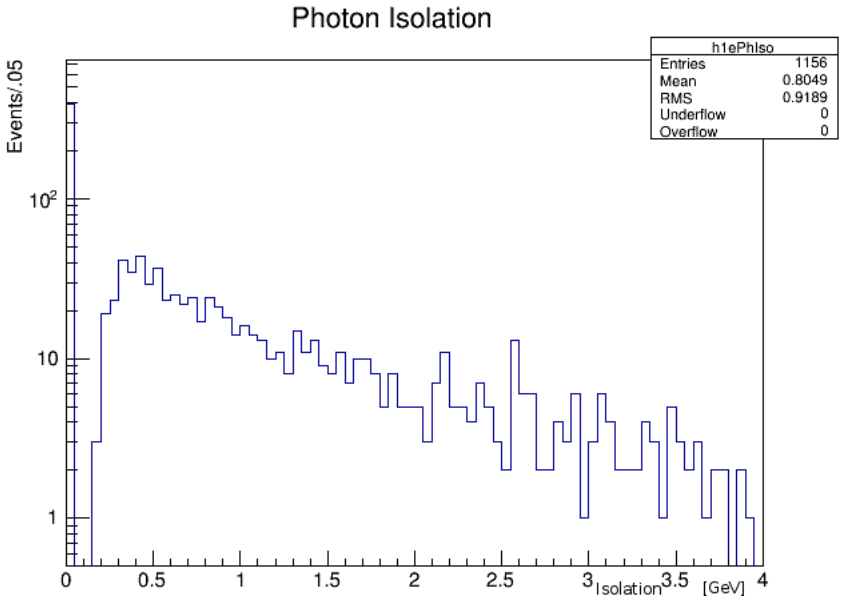

Figure 14: Photon Isolation for both lead and trail photons

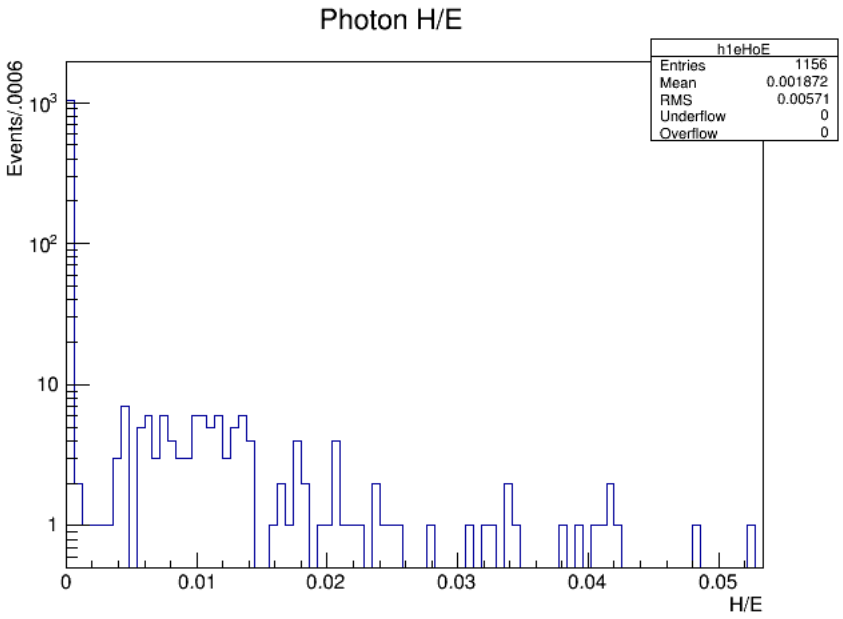

Figure 15: Photon H/E for both lead and trail photons

4.2 Candidate Electron

.

The electron sample is only required to pass an E_T >25 GeV cut and have an associated track. Unlike the photon objects, electrons are not required to be in the endcap. This can be seen by comparing the η distribution of the candidate electrons in Fig(17) to the η distributions of the two highest energy photons in Fig(10) and Fig(11).

Pileup is the product of non-interacting constituents of the colliding protons that hadronize in the direction of the endcaps. The η distribution Fig(17) of the candidate electrons is roughly uniform throughout the barrel and endcap.[7] This suggests that our sample does not pick up significant background from pileup in the endcaps.

[7]The barrel is the region where $|\eta|$ <1.44.

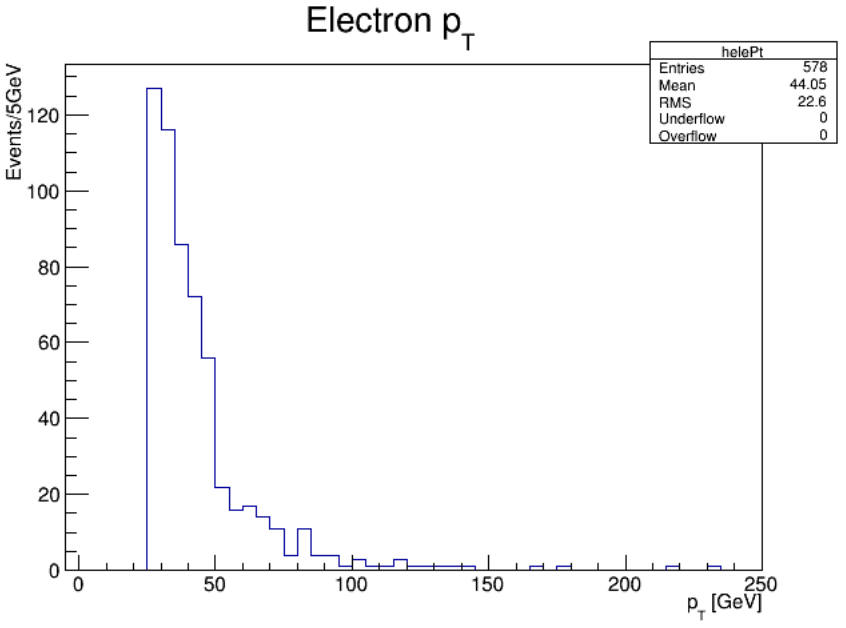

Figure 16: Electron p_T

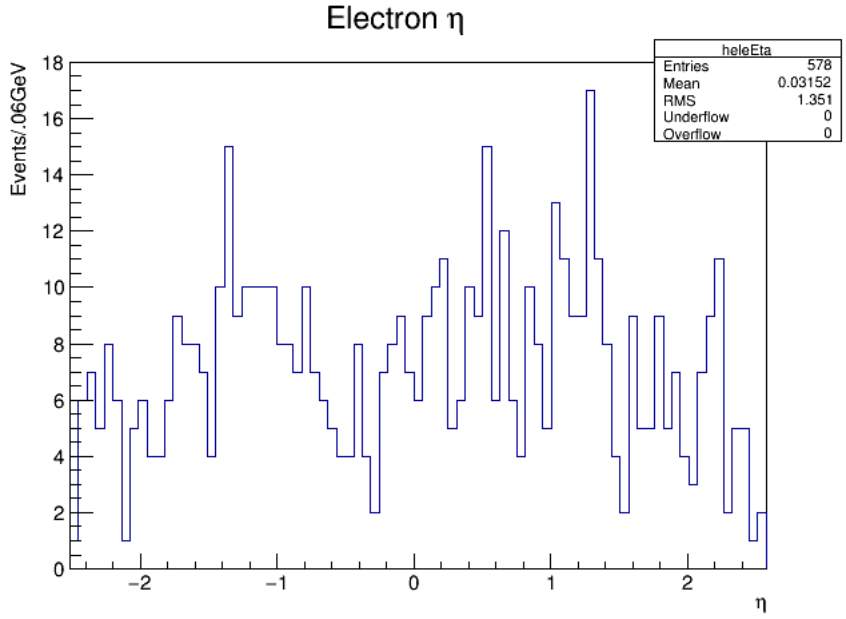

Figure 17: Electron η

4.3 Final Candidate Sample Size

.

Events are only selected if all objects (lead photon, trail photon, and electron) in the event pass the selection criteria outlined in their respective sections. This gives us a final candidate sample size of 578 events.

4.4 MET

.

Because of detector limitations, not all final state particles can be observed; in particular, those particles that interact only weakly. As a result, particles escape the detector leaving behind an imbalance in momentum in the direction transverse to the beam. This imbalance can be used to calculate a quantity known as Missing Transverse Energy (MET).

In hadron colliders, missing energy is only calculated using momentum in the transverse direction. High energy proton-proton collisions are collisions between the constituent quarks that make up the protons, where not all quarks interact during the collision. As a result, the final longitudinal momentum of the proton-proton collision cannot be precisely measured; however, this does not affect momentum transverse to the beam, which should have zero net final momentum.

The Missing Transverse Energy used in this analysis is more precisely defined as the negative vector sum of the p_T of all the particle flow particles in the event.[8]

$$M\vec{E}T = -\Sigma\vec{p_T} \tag{10}$$

[8]MET is used in many searches and measurements. An example of a use of MET is given in [17], but there are many others.

While energy is naturally a scalar quantity, MET defined in this way (10) is a vector. It is a measure of both the magnitude and direction of the imbalance of transverse momentum in the event.

Missing transverse energy (MET) quantifies the imbalance in momentum measured in each event. MET can result from weakly interacting particles escaping the detector, and is a key signature of this search; however, missing transverse energy is also the result of a finite resolution of our detector.

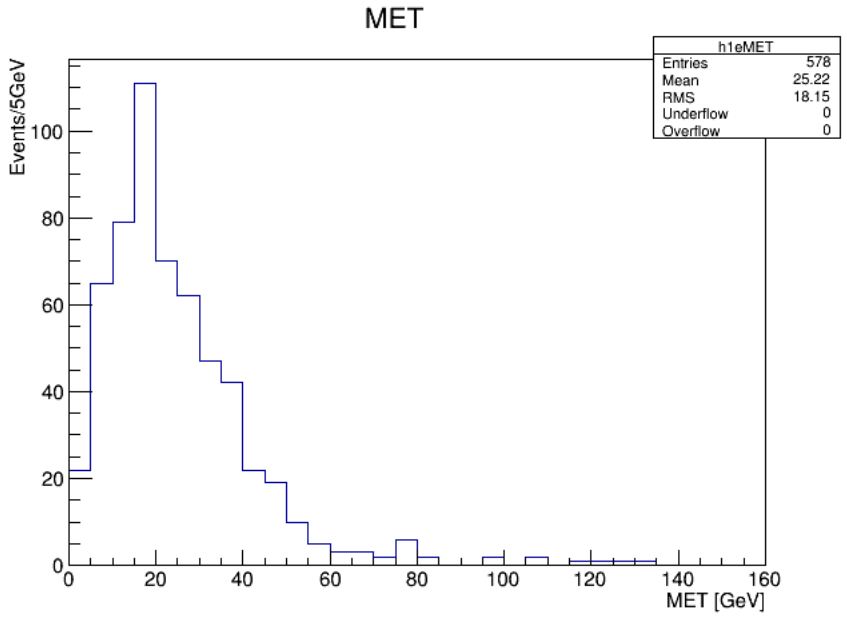

Figure 18: Candidate MET after applying Selection Criteria

5 Background Estimation

.

Background Standard Model physics is primarily dominated by QCD. In order to estimate MET that results from jets, we employ a technique similar to what is used in Ref[13]. This involves choosing a control sample – here dielectron events – whose distribution is characteristic of a distribution Fig(19) lacking real Missing Transverse Energy. The assumption being that a dielectron sample is dominated almost entirely by Z decays to two electrons, where the Z in these events likely rebounds off a jet. The measurement of the jet gives rise to the fake MET.

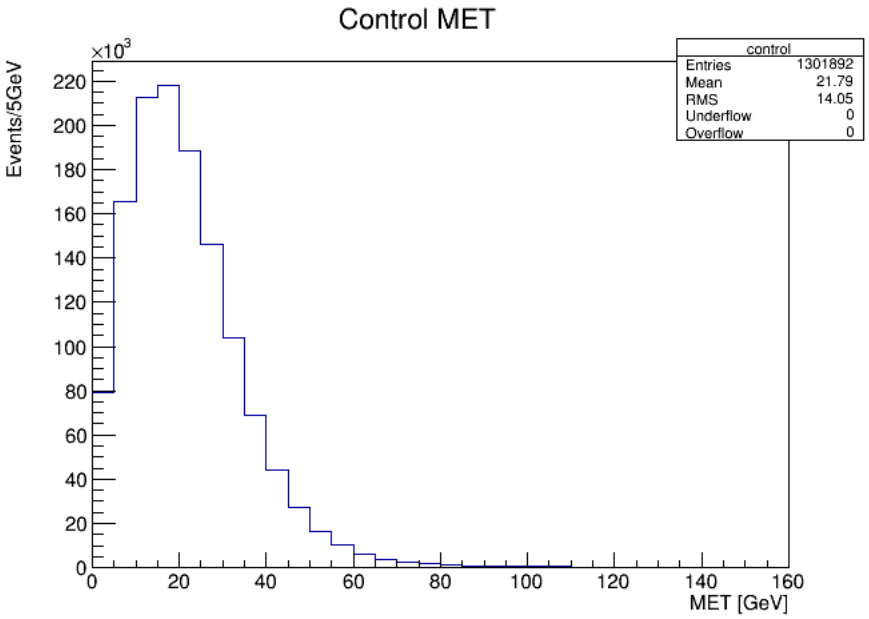

Figure 19: MET Distribution of dielectron control sample

5.1 System p_T

.

A total system p_T is calculated for each candidate event and control event indepen-

dently. Let these quantities be denoted as $p_{T_{cand}}$ and $p_{T_{control}}$. The candidate system p_T and the control system p_T are calculated as follows:

1) First decompose each object into its azimuthal cartesian (x,y) coordinates using the following map:

$$p_x = p_T \cos(\phi) \tag{11}$$

$$p_y = p_T \sin(\phi) \tag{12}$$

Where p_x and p_y are the momentums in the x and y direction respectively.
This produces the following momentum 2-vector $\vec{p}$ which lives in the azimuthal plane:

$$\vec{p} = (p_x, p_y) \tag{13}$$

Do this for every object in the event.

2) Take the vector sum of each object in the event.
For example, the system momentum 2-vector for the candidate sample:

$$\vec{p_{cand}} = \vec{p_{\gamma 1}} + \vec{p_{\gamma 2}} + \vec{p_e} \tag{14}$$

Where $\vec{p_{\gamma 1}}$, $\vec{p_{\gamma 2}}$, and $\vec{p_e}$ in Eqn(14) represent the 2-momentum for the lead energy photon, the trail energy photon, and the electron respectively.

3) Calculate the system p_T as the magnitude of the system 2-momentum.
Following the previous example, the $p_{T_{cand}}$ can be calculated as:

$$p_{T_{cand}} = mag(\vec{p_{\gamma 1}} + \vec{p_{\gamma 2}} + \vec{p_e}) \tag{15}$$

5.2 Weights

.

The weights are calculated from Eqn(16), where $weight[n]$ represents the value in the n^{th} bin of the histogram Ratio $\gamma\gamma e/ee$ in Fig(20). Further $p_{T_{cand}}[n]$ and $p_{T_{control}}[n]$ represent the value in the n^{th} bin of their respective histogram.[9]

$$weight[n] = \frac{p_{T_{cand}}[n]}{p_{T_{control}}[n]} \tag{16}$$

For example, with 5 GeV per bin, the number of events with a candidate system p_T equal to 100 GeV (which falls into the 20th bin) is equal to $p_{T_{cand}}[20]$. The number of events with a control system p_T equal to 100 GeV (20th bin) is equal to $p_{T_{control}}[20]$. The 20th bin of the weight histogram would be filled with $weight[20] = p_{T_{cand}}[20]/p_{T_{control}}[20]$. If there are 3 candidate events and 13 control events with p_T between 95-100 GeV, then the ratio is equal to $weight[20] = 3/13$.

[9]The system p_T histograms are normalized to 1 in order to account for the large difference in size between the candidate and control sample.

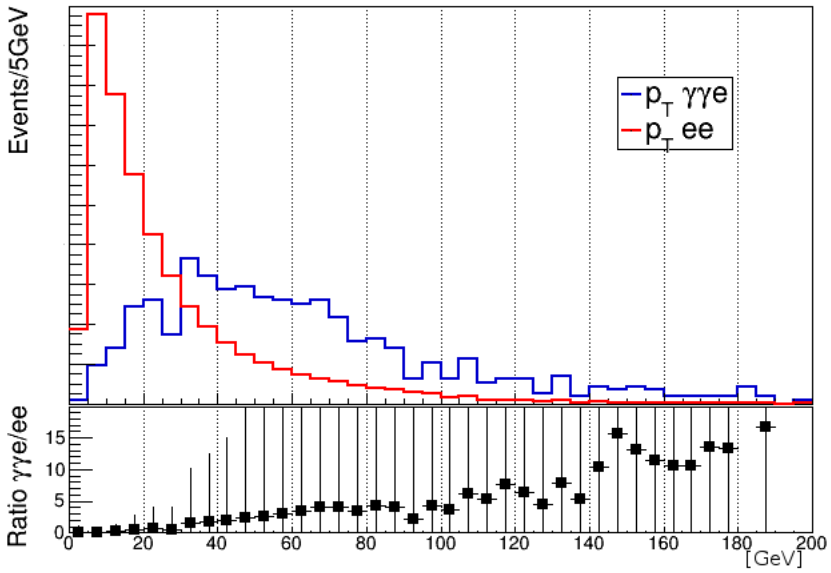

Figure 20: Candidate and Control System p_T (area normalized to 1)

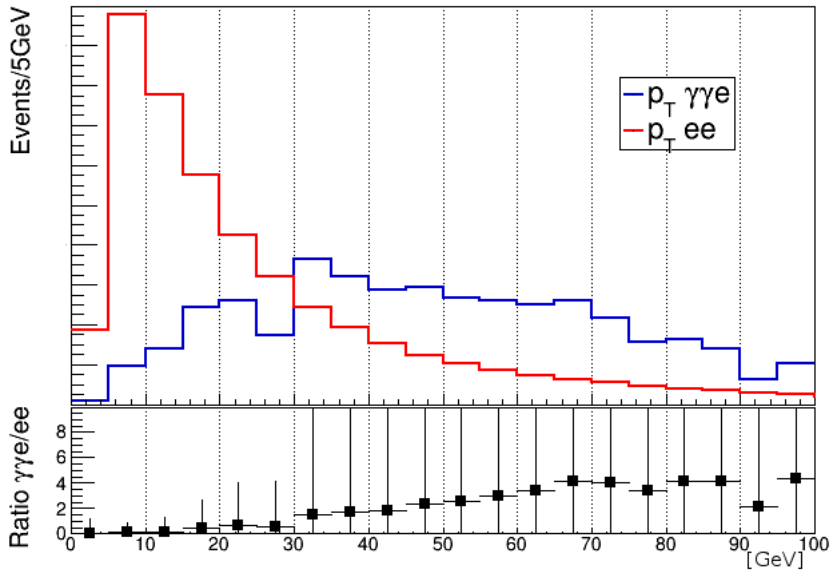

Figure 21: Candidate and Control System p_T (area normalized to 1)

5.3 The Reweighting

.

The goal is to produce the distribution that would be expected if there was no true

MET. The hypothesis is that the MET distribution of the dielectron control sample Fig(19) is dominated by Z decays to two electrons and no true MET. Using this hypothesis we can reweight the control sample using the ratio of the number of events in our candidate sample to the number of events in our control sample that have the same total system p_T.[10]

Explicitly, the process is as follows. If a event is in our dielectron control sample, calculate its system p_T. Add that event to the reweighted MET histogram, reweighting the entry using the weight corresponding to the calculated system p_T for that event. As an example (with 5 GeV per bin), assume an event that has a MET equal to 50 GeV and a system p_T equal to 100 GeV (the 20th bin). Fill the bin corresponding to 50 GeV (10th bin) in the MET histogram using $weight[20]$ as the weight for that histogram entry.

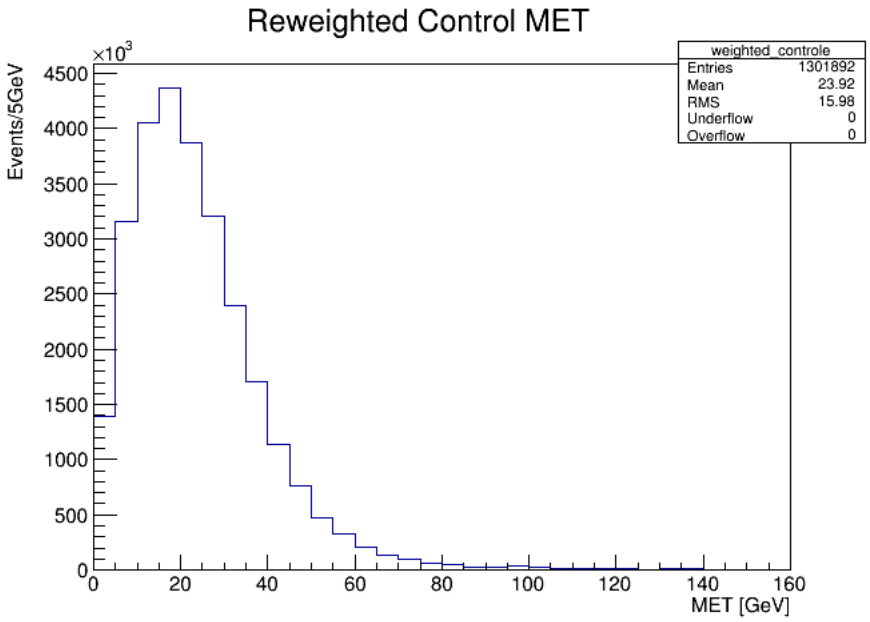

Figure 22: Reweighted MET distribution for dielectron control sample

[10]For example, if this ratio for a particular system p_T is close to 1, then this is indicative of a similar composition between our candidate sample and control sample (for events with that particular system p_T).

We produce a new plot Fig(22) by reweighting the MET of each event in the control sample using the ratio of events corresponding to that events system p_T. If the resulting reweighted MET distribution is similar to the original unweighted control MET, then this indicates that our candidate sample contains no real MET.

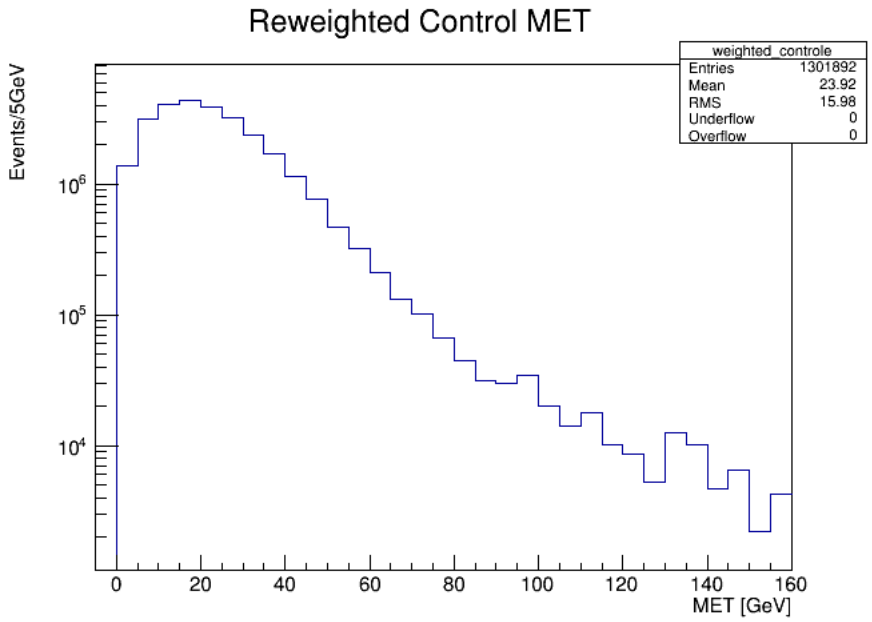

Figure 23: Logarithmic Scaling of Reweighted MET distribution for dielectron control sample

5.4 Systematic Uncertainty of MET Reweighting

.

The systematic uncertainty of our MET reweighting is estimated by generating 1000 different Ratio plots, where each bin in the Ratio plot is varied by a Gaussian distribution. The uncertainty of the Gaussian distribution is taken to be the statistical uncertainty σ defined by Eqn(17), where n is the number of candidate events and N is the number of control events in each bin of the normalized p_T of Fig(20). Both σ_n and σ_N are Poisson uncertainties for the candidate and control respectively.

$$\sigma = \frac{n}{N}\sqrt{(\frac{\sigma_n}{n})^2 + (\frac{\sigma_N}{N})^2} \tag{17}$$

The MET distribution is then reweighted using the 1000 different ratio plots as weights. Figure(24) is the fractional uncertainty per bin (where each bin corresponds to a 5 GeV increment of MET) produced by looping over every reweighted MET distribution for each bin and taking the 1σ standard deviation from the mean.

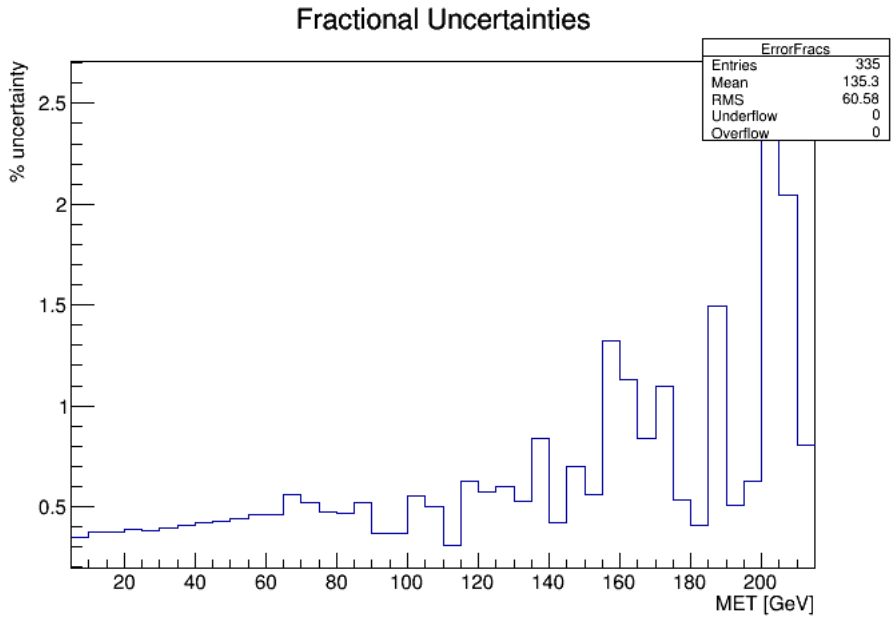

Figure 24: Plot of Fractional Uncertainties versus MET

6 Results

.

A total of 6 events are observed in the signal region for this analysis (MET>100 GeV), with an estimated QCD background of 8.02 coming from the dielectron distribution. We determine 95% confidence level upper limits on the electroweak neutralino-chargino production cross section shown in Fig(27). None of the six mass points in Fig(27) are excluded.

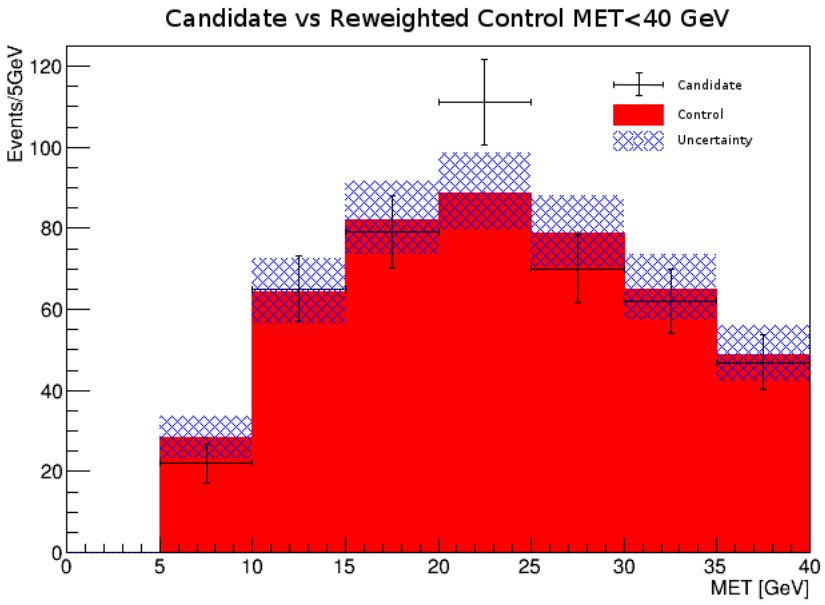

Figure 25: Comparison of the Reweighted Control MET to the candidate MET in the region MET<40 GeV

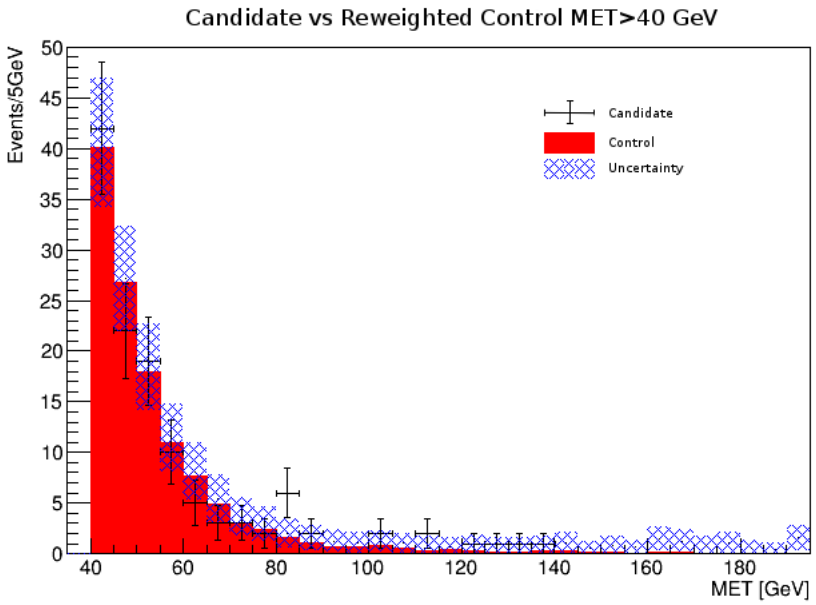

Figure 26: Comparison of the Reweighted Control MET to the candidate MET in the region MET>40 GeV

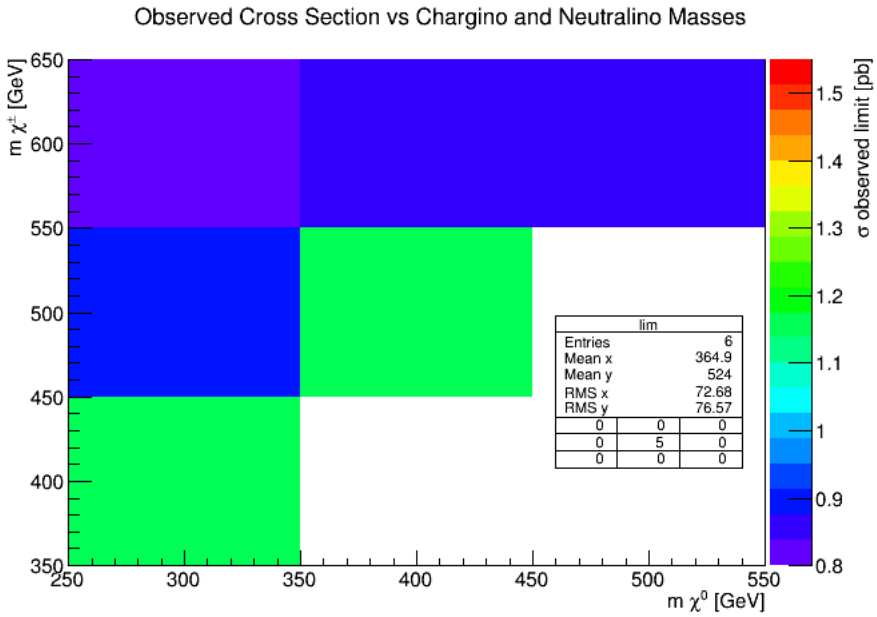

Figure 27: Observed Cross Section Limit

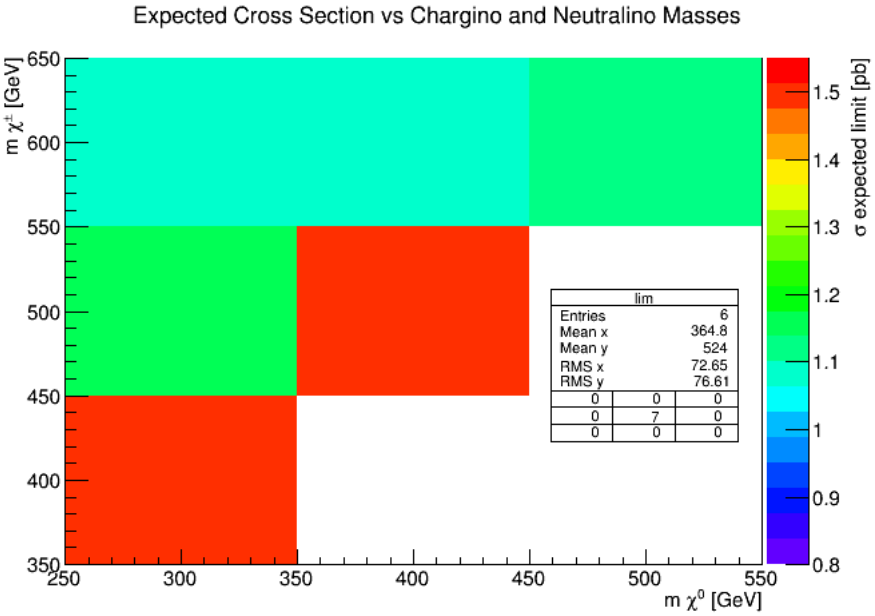

Figure 28: Expected Cross Section Limit

Table 4: Observed and Expected Cross Section Limits and corresponding Mass Points

$m_{\chi^\pm}$	m_{χ^0}	obs limit [pb]	exp limit [pb]
400	300	1.16	1.50
500	300	.89	1.15
500	400	1.15	1.49
600	300	.83	1.07
600	400	.85	1.10
600	500	.86	1.11

7 References

References

[1] Hinshaw, G.F., et.al., 2013, ApJS., 208, 19H

[2] NASA / WMAP Science Team. Universe Content 9yr Pie Chart. http://map.gsfc.nasa.gov/media/121236/index.html

[3] K.A. Olive et al. (Particle Data Group), Chin. Phys. C, 38, 090001 (2014).

[4] The dark matter of gravitational lensing. Massey, Kitching, Richard. http://arxiv.org/abs/1001.1739

[5] X-ray: NASA/CXC/CfA/M.Markevitch et al.; Optical: NASA/STScI; Magellan/U.Arizona/D.Clowe et al.; Lensing Map: NASA/STScI; ESO WFI; Magellan/U.Arizona/D.Clowe et al.

[6] Brauner. Spontaneous Symmetry Breaking and Nambu-Goldstone Bosons in Quantum Many-Body Systems. http://arxiv.org/abs/1001.5212

[7] *"Searches for electroweak neutralino and chargino production in channels with Higgs, Z, and W bosons in pp collisions at 8TeV"*. The CMS Collaboraton. doi : 10.1103/$PhysRevD$.90.092007

[8] *"Search for supersymmetry in events with a photon, a lepton, and missing transverse momentum in pp collisions at* $\sqrt{s}$ *=8 TeV"*. The CMS Collaboration. http://dx.doi.org/10.1016/j.physletb.2016.03.039

[9] The CERN Large Hadron Collider: Accelerator and Experiments. Volume 2. CERN. Geneva. 2009.

[10] Transverse Slice Through CMS. Image. $https$: $//www.phys.ksu.edu/reu2014/wabehn/index_files/image005.gif$

[11] Andrew Askew. Shower Width. http://home.fnal.gov/ askew/

[12] Brendan F Diamond. A Search for New Physics with a Three Photon Final State using the CMS Detector. 2015. p31-37.

[13] *"Search for supersymmetry in events with photons and missing transverse energy"*. The CMS Collaboration.

[14] Andrew Askew. ECAL Clustering. http://home.fnal.gov/ askew/

[15] Andrew Askew. Photon Masterclass Introduction. http://home.fnal.gov/ askew/

[16] Awes et al., NIM A311, p130-138.

[17] *"A Measurement of the W Boson Mass"*. D0 Collaboration. 1997.